nanomaterials

MDPI

Article

The Enhanced Red Emission and Improved Thermal Stability of $CaAlSiN_3:Eu^{2+}$ Phosphors by Using Nano-EuB_6 as Raw Material

Wen-Quan Liu [1], Dan Wu [2], Hugejile Chang [1], Ru-Xia Duan [1], Wen-Jie Wu [1], Guleng Amu [3], Ke-Fu Chao [1,*], Fu-Quan Bao [1] and Ojiyed Tegus [1,*]

1 Inner Mongolia Key Laboratory for Physics and Chemistry of Functional Materials, College of Physics and Electronic Information, Inner Mongolia Normal University, Hohhot 010022, China; seazuri@163.com (W.-Q.L.); criffchang@gmail.com (H.C.); ruxia1028@163.com (R.-X.D.); 15248127843@163.com (W.-J.W.); b.fuquan@imnu.edu.cn (F.-Q.B.)

2 School of Physical Science and Technology, & Inner Mongolia Key Lab of Nanoscience and Nanotechnology, Inner Mongolia University, Hohhot 010021, China; wudan20101203@163.com

3 Department of physics and electrical engineering, Xilingol Vocational College, Xilinhot 0026000, China; amgl15947298308@163.com

* Correspondence: phyerick@imnu.edu.cn (K.-F.C.); tegusph@imnu.edu.cn (O.T.); Tel.: +86-471-4392576 (K.-F.C.)

Received: 22 December 2017; Accepted: 22 January 2018; Published: 25 January 2018

Abstract: Synthesizing phosphors with high performance is still a necessary work for phosphor-converted white light-emitting diodes (W-LEDs). In this paper, three series of $CaAlSiN_3:Eu^{2+}$ (denoted as CASN:Eu^{2+}) phosphors using Eu_2O_3, EuN and EuB_6 as raw materials respectively are fabricated by under the alloy precursor normal pressure nitridation synthesis condition. We demonstrate that CASN:Eu^{2+} using nano-EuB_6 as raw material shows higher emission intensity than others, which is ascribed to the increment of Eu^{2+} ionic content entering into the crystal lattice. An improved thermal stability can also be obtained by using nano-EuB_6 due to the structurally stable status, which is assigned to the partial substitution of Eu–O (Eu–N) bonds by more covalent Eu–B ones that leads to a higher structural rigidity. In addition, the W-LEDs lamp was fabricated to explore its possible application in W-LEDs based on blue LEDs. Our results indicate that using EuB_6 as raw materials can provide an effective way of enhancing the red emission and improving the thermal stability of the CASN:Eu^{2+} red phosphor.

Keywords: alloy precursors; nitride; $CaAlSiN_3:Eu^{2+}$red phosphor; nano-EuB_6

1. Introduction

White light-emitting diodes (W-LEDs) are considered as the next-generation solid-state lighting system due to the high luminous efficiency, long operation time, reliability environmental friendliness [1–3]. The traditional way used to obtain white light is combing blue InGaN LEDs chip with the yellow phosphor $Y_3Al_5O_{12}:Ce^{3+}$ (YAG:Ce^{3+}). However, using a single yellow phosphor leads to low color rendering index (Ra < 80) due to the insufficient red component in the spectra, making them unsuitable for high-quality "warmer" white lighting [4–7]. Therefore, a red emitting phosphor is thus essentially needed to enhance the red spectral part to achieve much higher color rendering indices.

Currently, several red emitting phosphors attract much attention and are pervasively studied due to the property of effectively enhancing the color rendition, such as $M_2Si_5N_8:Eu^{2+}$ (M = Ca, Ba, Sr) [8–11], $SrLiAl_3N_4:Eu^{2+}$ [12–15] and CASN:Eu^{2+} [16–19]. Among the above red phosphors, the emission of Eu^{2+} in $CaAlSiN_3$ host locates in deep red region and possesses the advantages of good thermal stability, reliability and high quantum efficiency, which make it superior to others.

There are many preparation methods in fabricating CASN:Eu^{2+} red phosphors each has its own shortcomings. Commonly, the metal and rare earth nitrides are used as raw materials in preparing CASN:Eu^{2+} red phosphors they have to be operated in glove box because nitride compounds are unstable, decomposable and oxidizable in the air hence, the ideas of inhibiting certain disintegrating process put higher requirements to the experimental equipment and additional standards of higher temperature ($\geq$1800°) and pressure ($\geq$1 MPa) [20,21]. For example, experimental expensive and yield small amounts of outcome when it comes to spark plasma sintering (SPS) process [22,23] and self-propagating high temperature synthesis (SHS) procedures [19,24], therefore, it is difficult to be carried out in manufacturing. In contrast, the alloy precursor normal pressure nitridation process is easier to operate rested upon high active alloy without high temperature ($\geq$1800°) and high pressure ($\geq$1 MPa) requirement, whereas the oxidation of the raw material is difficult to avoid. Higher oxygen content in raw materials necessitates it to be processed with oxidation-reduction treatment. To this end, several very simple methods like gas reduction nitridation (GRN) method [25,26] and carbothermal reduction and nitridation (CTRN) method [27,28] are applied to the preparation of CASN:Eu^{2+} nitride materials. However, the obtained product contained impurities of unreacted CaO and excess C powders. Combined with, alloy precursor and non-oxygen raw materials will help improve luminescence performance of CASN:Eu^{2+} series nitride phosphors.

In this paper, a high performance CASN:Eu^{2+} red phosphors, using nano-EuB_6 as raw materials, were obtained by alloy precursor normal pressure nitridation. The above red phosphor exhibits an enhanced red emission and improved thermal stability, which permits it to be superior to the common used CASN:Eu^{2+} phosphors using Eu_2O_3 and EuN as raw materials. The possible performance of the red phosphor in W-LED was also investigated.

2. Experimental

2.1. Sample Preparation

The powder samples were synthesized by the alloy precursor normal pressure nitridation method in a high temperature tubular furnace with the raw materials of CaSi alloy, AlN (99.5%), Eu_2O_3 (99.99%), EuN (99.9%) and nano-EuB_6. EuB_6 is a typical semimetal material, Eu atoms are centered as an octahedron composed of six rigidly bound lighter atoms of boron. Thus, it has rich structure and excellent physical and chemical properties [29,30]. The energy bands of the EuB_6 can be considered to be formed by orbital interactions between Eu^{2+} and $B_6{}^{2-}$ clusters. Synthesized nano-EuB_6 was reported method by the Bao et al. [31]. Eu_2O_3 (99.99%) and $NaBH_4$ (99.0%) mixed in an agate mortar for 30 min. Then the mixtures were put into a quartz tube and placed in the resistance furnace at a reaction temperature in the range from 1150 °C to 1200 °C for 2 h. Therein CaSi alloy is sintered by reactants Ca (99.5%), Si (99.999%) through arc melting process in Ar gas. The resulting mixtures that using Eu_2O_3 and EuN as raw materials were heated at 1550 °C for 4 h under a 200 mL min^{-1} N_2 (99.999%) and 20 mL min^{-1} H_2 (99.999%) reducing atmosphere with a constant flow rate 100 mL/min while that using nano-EuB_6 were heated at 1550 °C for 4 hundred a 200 mL min^{-1} N_2 (99.999%). Finally, the samples were cooled to room temperature in the furnace and ground again for the following characterization.

2.2. Measurements and Characterization

The microstructure and chemical composition of powders were imaged and measured by using a scanning electron microscopy (SEM, Hitachi S-3400N, Hitachi High-Tech Fielding Corporation, Tokyo, Japan) and X-ray energy dispersive spectrometer (EDS, Hitachi, Tokyo, Japan) equipment. The crystal structure was determined via X-ray powder diffraction (XRD, Philip PW1830 with Cu Kα radiation operating at 30 kV and 30 mA, Amsterdam, The Netherlands) at room temperature. The X-ray photoelectron spectroscopy (XPS) spectra were carried out with the X-ray photoelectron spectrometer (ESCALAB 250, Thermo Fisher Scientific, Loughborough, UK) using Al $K\alpha_1$ radiation at 15 kV and 10 mA. The emission spectra were measured by a Hitachi F4600 fluorescence spectrophotometer

(Hitachi, Tokyo, Japan). The temperature-dependent PL spectra were also carried out on Hitachi F-7000 spectrometer (Hitachi, Tokyo, Japan) with an external heater.

A white LED was fabricated by combining a blue-LED chip (455 nm) with commercial green phosphor G3537, the as-synthesized CASN:Eu^{2+}. The optical properties of the fabricated W-LEDs were measured using sphere spectroradiometer system (LHS-1000, Everfine Co., Hangzhou, China). The working bias voltage and current of LEDs are respectively 3.4 V and 20 mA. All the measurements were conducted at room temperature unless mentioned specially.

3. Results and Discussion

3.1. Structure Characterization

The XRD pattern and the crystal structure of the used nano-EuB_6 were shown in Figure 1a. The morphologies of nano-EuB_6, CaSi alloy powder and the as-synthesized samples CASN:Eu^{2+}@Eu_2O_3, CASN:Eu^{2+}@EuN, as well as CASN:Eu^{2+}@EuB_6 were observed by the SEM image in Figure 1b–f. The central particle size of the used nano-EuB_6 is around 200~300 nm. One can find that there exists an obvious agglomeration in CASN:Eu^{2+}@Eu_2O_3, whose particles is relatively bigger and irregular than those of CASN:Eu^{2+}@EuN and CASN:Eu^{2+}@EuB_6.

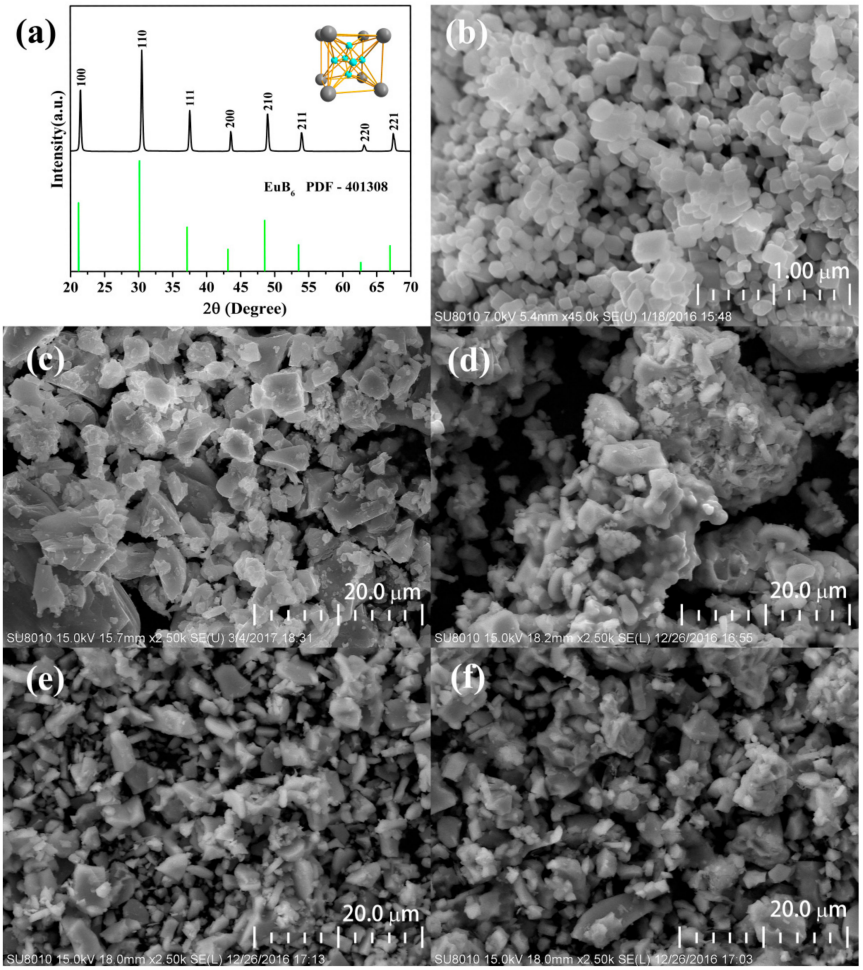

Figure 1. XRD patterns of (**a**) nano-EuB_6 and the SEM images of (**b**) nano-EuB_6; (**c**) CaSi alloys; (**d**) $Ca_{0.94}AlSiN_3$:0.06Eu^{2+}@Eu_2O_3; (**e**) $Ca_{0.94}AlSiN_3$:0.06Eu^{2+}@EuN; and (**f**) $Ca_{0.94}AlSiN_3$:0.06Eu^{2+}@EuB_6.

The EDS analytical data of CaSi alloys, CASN:Eu^{2+}@Eu_2O_3, CASN:Eu^{2+}@EuN and CASN:Eu^{2+}@EuB_6 were listed in Table 1. One can find that there exists a small amount of oxygen

in CaSi alloys and it cannot be avoided effectively. The EDS analysis reveals that CASN:Eu^{2+}@EuB_6 contains least oxygen while the maximum oxygen content in CASN:Eu^{2+}@Eu_2O_3. The possible explanation of this phenomenon is that Eu_2O_3 is not fully reduced by local substances during sintering operations. It should be mentioned that the powders synthesized by EuN as the raw material are easier to be oxidized due to its high activity. Comparatively, the EuB_6 has the properties of physically and chemically stable, which prevents it from oxidation. The small amount of oxygen impurities in CASN:Eu^{2+}@EuB_6 are also attributed to the CaSi alloy, which could be reduced under a reducing atmosphere.

Table 1. EDS analytical data of CaSi alloys, $Ca_{0.94}AlSiN_3$:0.06Eu^{2+}@Eu_2O_3, $Ca_{0.94}AlSiN_3$:0.06Eu^{2+}@EuN and $Ca_{0.94}AlSiN_3$:0.06Eu^{2+}@EuB_6.

Element (wt %)	B	N	O	Al	Si	Ca	Eu
CaSi alloys	— —	— —	4.28	— —	59.39	36.33	— —
$Ca_{0.94}AlSiN_3$:0.06Eu^{2+}@Eu_2O_3	— —	21.52	6.19	18.05	28.53	22.53	3.26
$Ca_{0.94}AlSiN_3$:0.06Eu^{2+}@EuN	— —	36.33	2.78	18.04	23.83	15.76	3.25
$Ca_{0.94}AlSiN_3$:0.06Eu^{2+}@EuB_6	5.17	25.56	1.95	18.27	26.49	19.32	3.27

The XRD patterns of three series CASN:Eu^{2+} (x = 0.01, 0.02, 0.03,0.04, 0.06) phosphors using Eu_2O_3, EuN and EuB_6 as raw materials, labeled as CASN:Eu^{2+}@Eu_2O_3, CASN:Eu^{2+}@EuN as well as CASN:Eu^{2+}@EuB_6 respectively, are shown in Figure 2 the standard XRD pattern of $CaAlSiN_3$ (PDF-390747) is also shown for comparison. As illustrated in Figure 2, the diffraction peaks are predominantly identified as $CaAlSiN_3$ phase and crystallize in the orthorhombic space group $Ccm2_1$. It should be noted that the impurity phases, Ca_2SiO_4 (PDF-110585) and AlN (PDF-871054) in CASN:Eu^{2+}@Eu_2O_3 and CASN:Eu^{2+}@EuN as well as an extra phase BN (PDF-090012) in CASN:Eu^{2+}@EuB_6 are also identified, as shown in Figure 2a–c. Since the synthesis conditions of CASN:Eu^{2+} phosphors need a high requirement for installations, the impurity phases are unavoidable during the sinter process. In our work, the impurity phase Ca_2SiO_4 emerged during the preparation of CaSi alloy due to the oxidized process and it is expected to increase with the appearance of a rich oxygen source Eu_2O_3, which is confirmed by the more intense peak intensity in CASN:Eu^{2+}@Eu_2O_3 than that in CASN:Eu^{2+}@EuN and CASN:Eu^{2+}@EuB_6. The above result is also consistent with the ratios of N/O in different samples that measured by EDS (see Table 1). For the impurity phase AlN, its precise stoichiometric ratio in the reaction can hardly be determined due to its low solubility in $CaAlSiN_3$, which results in the redundant AlN [32,33]. It can be found from Figure 3 that the main diffraction peaks of $CaAlSiN_3$ in the range of 30–40° shift to a low degree with the increase of Eu^{2+} ion concentration in CASN:Eu^{2+}@EuB_6, which could be ascribed to be the substitution of larger B^{2-} (1.40 Å, CN = 4) for smaller N^{3-} (1.32 Å, CN = 4) [17]. In CASN:Eu^{2+}@EuB_6, the diffraction peaks at 2θ = 33.5° is superposed by AlN and BN, which are formed within the reaction between B and N_2 (or AlN).

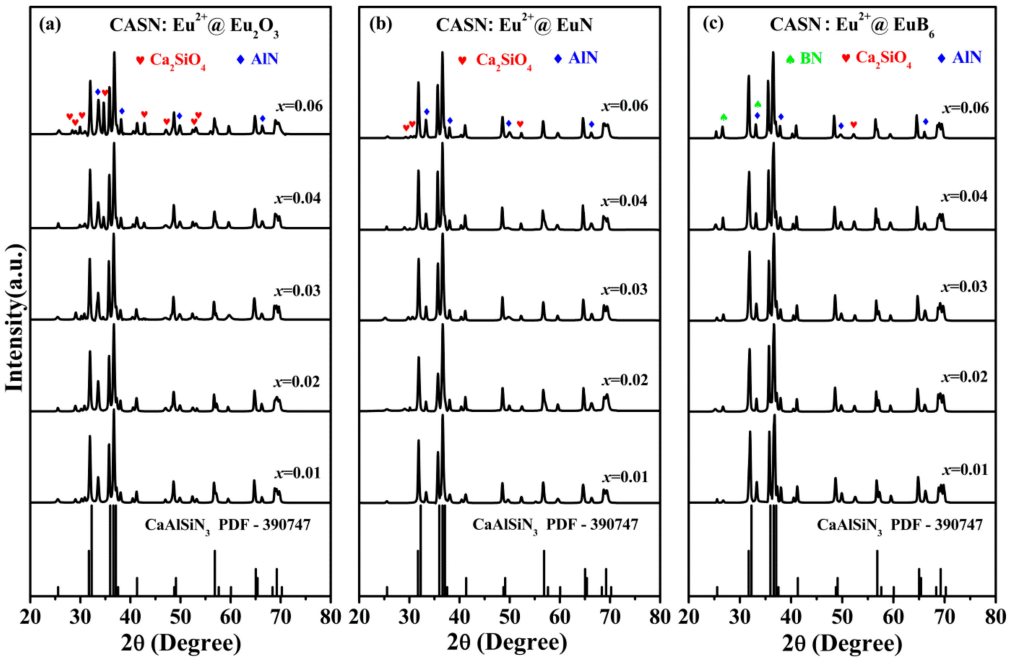

Figure 2. XRD patterns of three nitride red phosphors using different raw materials (**a**) CASN:Eu^{2+}@Eu_2O_3; (**b**) CASN:Eu^{2+}@EuN and (**c**) CASN:Eu^{2+}@EuB_6.

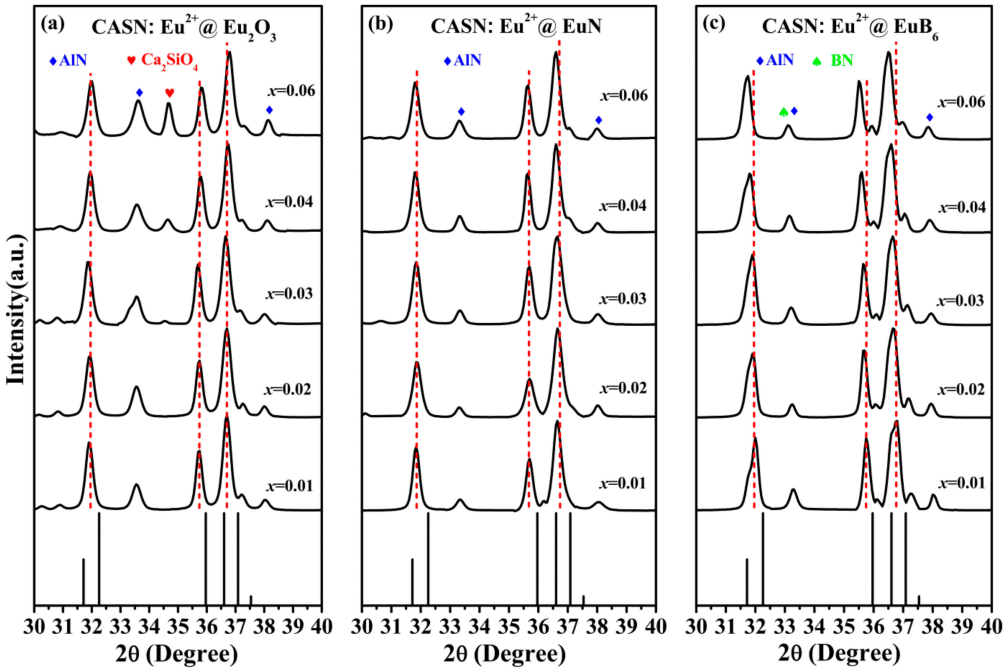

Figure 3. The major XRD patterns of three nitride red phosphors in the range of 30–40°; (**a**) CASN:Eu^{2+}@Eu_2O_3; (**b**) CASN:Eu^{2+}@EuN and (**c**) CASN:Eu^{2+}@EuB_6.

3.2. XPS Analysis

The XPS measurement was conducted to study the local valence state of each element. The XPS spectra of Eu_{3d} in CASN:Eu^{2+}@Eu_2O_3 (black line), CASN:Eu^{2+}@EuN (blue line), as well as CASN:Eu^{2+}@EuB_6 (red line) were shown in Figure 4. According to the certain references [34,35], the bands peaking at 1165.27 eV and 1135.86 eV in Eu_{3d} XPS spectra correspond to $Eu^{3+}(3d_{3/2})$ and $Eu^{3+}(3d_{5/2})$ respectively, while that peaking at 1155.22 eV and 1125.02 eV are attributed to $Eu^{2+}(3d_{3/2})$

and $Eu^{2+}(3d_{5/2})$. In the samples of CASN:Eu^{2+}@EuN and CASN:Eu^{2+}@EuB_6, there exist the bands of $Eu^{3+}(3d_{3/2})$, $Eu^{2+}(3d_{3/2})$, $Eu^{3+}(3d_{5/2})$, $Eu^{2+}(3d_{5/2})$, while in CASN:Eu^{2+}@Eu_2O_3, the bands of $Eu^{3+}(3d_{5/2})$ dominate the spectrum. Comparative result confirms that the peak intensity ratio of Eu^{2+} and Eu^{3+} are identical with its content ratio in EuN and EuB_6 doped (see Table 2). The observation shows that Eu^{2+} content in CASN:Eu^{2+}@EuN or CASN:Eu^{2+}@EuB_6 is nearly the same and both of them are higher than that in CASN:Eu^{2+}@Eu_2O_3.

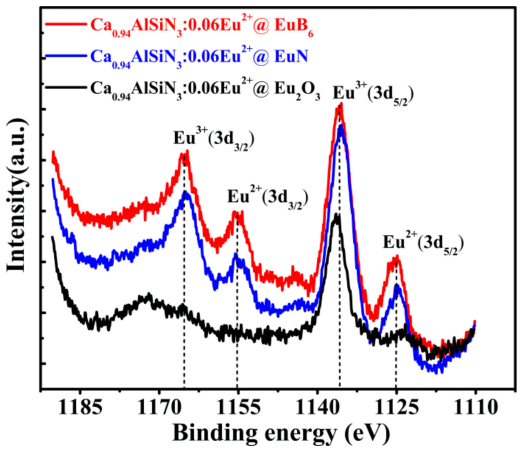

Figure 4. The XPS spectra of Eu_{3d} in $Ca_{0.94}AlSiN_3$:0.06Eu^{2+}@Eu_2O_3 (black line), $Ca_{0.94}AlSiN_3$: 0.06Eu^{2+}@EuN (blue line) and $Ca_{0.94}AlSiN_3$: 0.06 Eu^{2+}@EuB_6 (red line).

Table 2. Intensity ratios of Eu^{2+} /Eu^{3+} in $Ca_{0.94}AlSiN_3$:0.06Eu^{2+}@Eu_2O_3, $Ca_{0.94}AlSiN_3$:0.06Eu^{2+}@EuN and $Ca_{0.94}AlSiN_3$:0.06Eu^{2+}@EuB_6.

XPS Measurements	Intensity of Eu^{2+}	Intensity of Eu^{3+}	Eu^{2+}/Eu^{3+}
$Ca_{0.94}AlSiN_3$:0.06Eu^{2+}@EuN($3d_{3/2}$)	0.8847	0.9333	9.48/10
$Ca_{0.94}AlSiN_3$:0.06Eu^{2+}@EuN($3d_{5/2}$)	0.8596	0.9854	8.72/10
$Ca_{0.94}AlSiN_3$:0.06Eu^{2+}@EuB_6($3d_{3/2}$)	0.9166	0.9633	9.52/10
$Ca_{0.94}AlSiN_3$:0.06Eu^{2+}@EuB_6($3d_{5/2}$)	0.8817	1. 0000	8.82/10

Figure 5 shows the XPS spectra of N_{1s} and O_{1s} in CASN:Eu^{2+} samples series. The N_{1s} spectra, it can also be deconvoluted into two peaks: N–Ca (green line), N–Si (blue line) and N–Al (Cyan line) bonds. The content of N_{1s} that corresponds to N–Si bond in CASN:Eu^{2+}@EuB_6 is much higher than that in CASN:Eu^{2+}@Eu_2O_3 and CASN:Eu^{2+}@EuN at the same Eu doping level. It was reported that the binding energy of N_{1s} that correspond to N-B (magenta line) bond was around 397.6~398.5 eV [36,37]. One can find from the XRD data that there exists the impurity phase of BN in CASN:Eu^{2+}@EuB_6 sample. Therefore, it can be concluded that the peak intensity at the lower binding energy is the combined result of N–Si and N–B bonds. For the O_{1s} spectra can be deconvoluted into two peaks: O–Si (blue line) and O–Ca (green line) bonds. One can find that the peak intensity of the lower binding energy, which corresponds to O–Ca bond, has the minimum in CASN:Eu^{2+}@EuB_6 while has the maximum in CASN:Eu^{2+}@Eu_2O_3. It can be concluded from the XRD data that the existence of the impurity phase of $CaSiO_4$ is the main factor for the formation of O–Si and O–Ca bonds. Additionally, it can be found from the EDS results that oxygen content in CASN:Eu^{2+}@EuB_6 was significantly less than that in CASN:Eu^{2+}@Eu_2O_3 and CASN:Eu^{2+}@EuN.

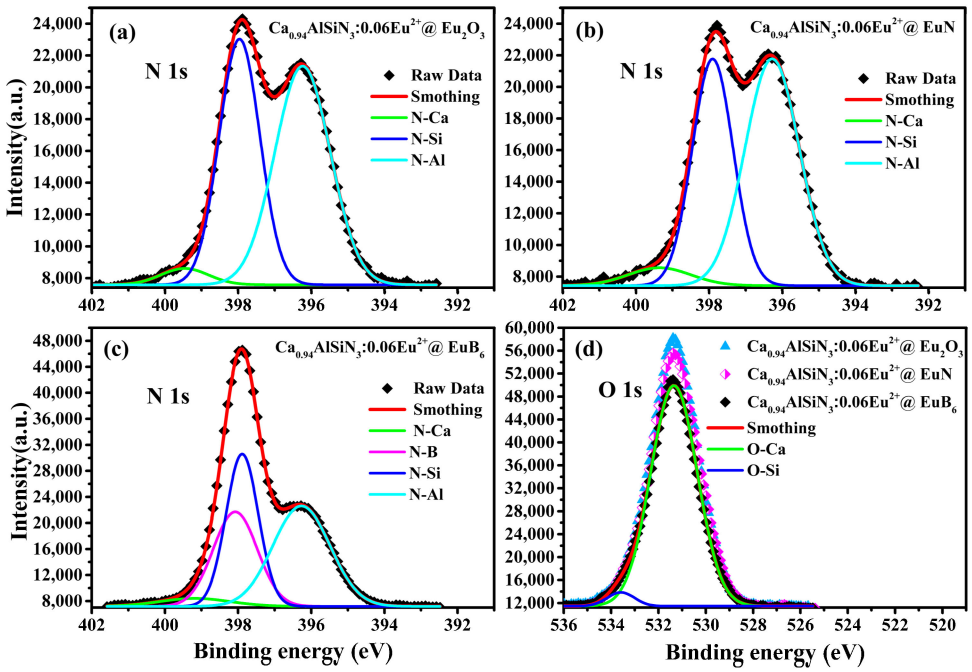

Figure 5. The XPS spectra of O_{1s} and N_{1s} $Ca_{0.94}AlSiN_3$:0.06Eu^{2+}@Eu_2O_3, $Ca_{0.94}AlSiN_3$:0.06Eu^{2+}@EuN and $Ca_{0.94}AlSiN_3$:0.06Eu^{2+}@EuB_6.

3.3. Photoluminescence Properties

The emission spectra of three groups of CASN:Eu^{2+}@Eu_2O_3, CASN:Eu^{2+}@EuN as well as CASN:Eu^{2+}@EuB_6 (x = 0.01, 0.02, 0.03, 0.04, 0.06) phosphors under 460 nm blue light excitation are shown in Figure 6. Upon the introduction of Eu^{2+} ion, the emission band attributed to the $5d \rightarrow 4f$ transition of Eu^{2+} ion dominates the spectra in all series of samples. One can find from Figure 6a–c that the emission intensity of Eu^{2+} ion in each group reaches its maximum value at x = 0.03, beyond which it starts to decrease due to the concentration quenching among Eu^{2+} ions. It should be noted that the emission intensity of Eu^{2+} ion in CASN:Eu^{2+}@EuB_6 is stronger than that in CASN:Eu^{2+}@EuN and CASN:Eu^{2+}@Eu_2O_3.

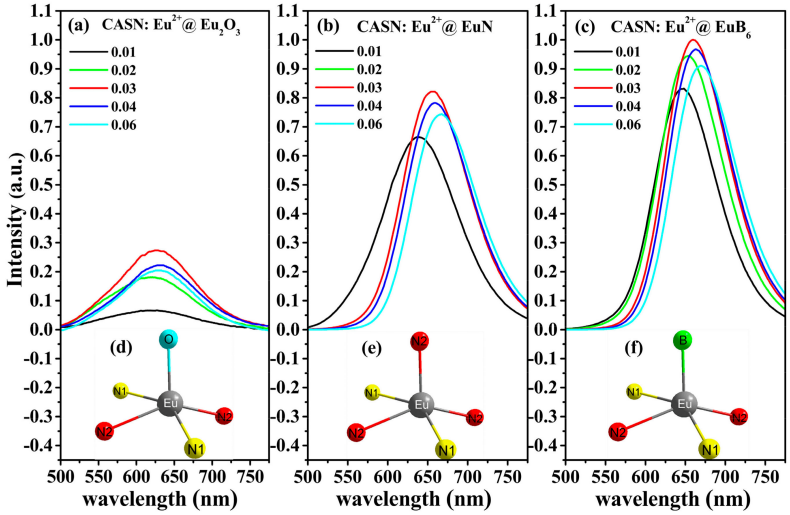

Figure 6. Photoluminescence spectra and crystallographic environments around Eu^{2+} ions of three series of nitride red phosphors using different raw materials (**a**) CASN:Eu^{2+}@Eu_2O_3; (**b**) CASN:Eu^{2+}@EuN; (**c**) CASN:Eu^{2+}@EuB_6; (**d**) $EuN_2^{I}N_2^{II}O$; (**e**) $EuN_2^{I}N_3^{II}$ and (**f**) $EuN_2^{I}N_2^{II}B$ phosphors with various content x (x = 0.01, 0.02, 0.03, 0.04, 0.06).

Under 460 nm blue light excitation, the emission peaks of CASN:Eu^{2+}@Eu_2O_3 fall in the scope of 621~636 nm while that of CASN:Eu^{2+}@EuN as well as CASN:Eu^{2+}@EuB_6 are in 640~668 nm, 648~670 nm, respectively. At the same Eu^{2+} doping concentration, the emission wavelength in CASN:Eu^{2+}@EuB_6 series is longer than that in CASN:Eu^{2+}@EuN (as shown in Figure 7a,b).

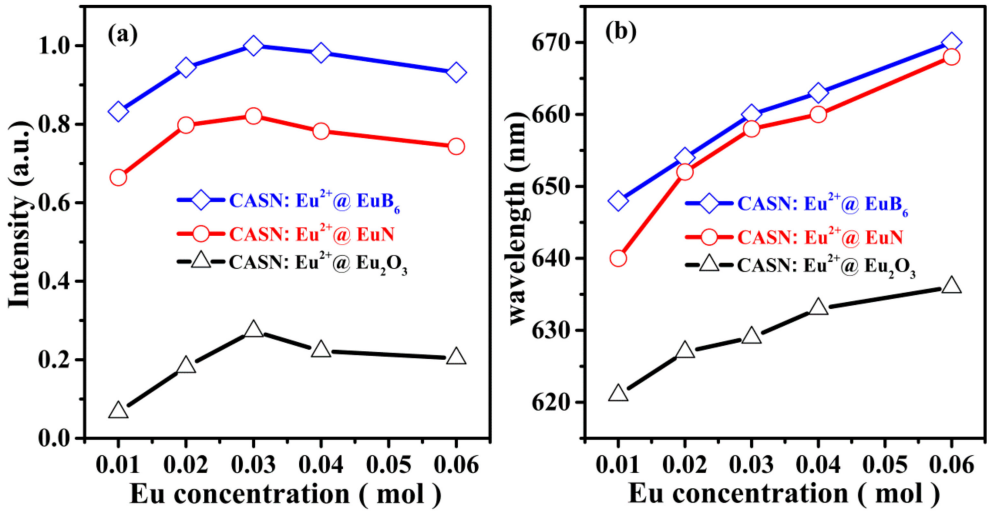

Figure 7. Dependence of emission intensity (**a**) and peak position (**b**) of CASN:Eu^{2+}@Eu_2O_3 (black line), CASN:Eu^{2+}@EuN (blue line) and CASN:Eu^{2+}@EuB_6 (red line) phosphors with various Eu^{2+} concentration (x = 0.01, 0.02, 0.03, 0.04, 0.06).

The XPS spectra reveal that Eu^{2+} content in both CASN:Eu^{2+}@EuN and CASN:Eu^{2+}@EuB_6 is higher than that in CASN:Eu^{2+}@Eu_2O_3. The amounts of O–Si, O–Ca bonds will decline accompanied by the increase of N-Si bond with the decrease of oxygen content in host materials, as a result, it affects the crystal field, which results in the split of Eu^{2+} energy levels. The position of the 5*d* emission band of the Eu^{2+} ions at lower energy (longer wavelength) is attributed to the influence of highly covalent bonding of Eu-*X* (*X* = N, B, O) and high crystal field strength. The reduction of crystal field strength around the Eu^{2+} ion in CASN:Eu^{2+}@Eu_2O_3 leads to a blue shift. However, under the influence of crystal field, the emission spectra have a larger red shift in CASN:Eu^{2+}@EuN and CASN:Eu^{2+}@EuB_6. This is caused by the shrinkage of $5d \rightarrow 4f$ energy level spacing [38].

Particularly, in the series of CASN:Eu^{2+}@EuB_6, with B^{2-} ions incorporating into the host lattice of $CaAlSiN_3$, they substitute N^{3-} and O^{2-} ions through a pattern of $EuN_2^{I}N_3^{II} \rightarrow EuN_2^{I}N_2^{II}B$ (see Figure 6f) [39] then, a red shift in the spectrum was expected due to the changed crystal strength. Moreover, the Eu–N bond length critically affects the emission wavelength of nitride phosphors. Therefore, we believe that according to the above schematic pattern the length of the Eu–B bonds is longer than that of the Eu–N bonds (see Figure 6e,f). In addition, the metal cation ratio in $CaAlSiN_3$ is Ca:Al:Si = 1:1:1, in which Ca and Al/Si occupied on the 4a and 8b sites in the space group of $Ccm2_1$, respectively [25,32]. In the series of CASN:Eu^{2+}@EuB_6, the decrease of oxygen content can prevent the formation of Ca_2SiO_4 and increase the content of occupation Ca ions, which can also lead to the improvement of emission intensity. Since the three series of samples have the same Eu^{2+} doping level thus the higher luminescence performance of CASN:Eu^{2+}@EuB_6 indicates that Eu^{2+} ions content in the host lattice has changed the crystal environment and the site occupancy.

3.4. Thermal Stability Analysis

A stable emission intensity at the elevated temperature, typically at 150 °C or even higher for high-power application is a basic requirement for phosphors converted W-LEDs thus the phosphors must have small thermal quenching to maintain the long lifetime of LED devices. In order to

evaluate the influence of the temperature on the luminescence, the temperature-dependent PL intensities of the as-prepared $Ca_{0.97}AlSiN_3$:0.03Eu^{2+}@Eu_2O_3, $Ca_{0.97}AlSiN_3$:0.03Eu^{2+}@EuN as well as $Ca_{0.97}AlSiN_3$:0.03Eu^{2+}@EuB_6 were given in Figure 8. The temperature–dependent PL intensities of YAG:0.06Ce^{3+} phosphor were also shown for comparison. It can be easily observed that all the above four phosphors exhibit thermal quenching in different degrees with temperature increasing from 30 °C to 210 °C. In addition, one can find that as the temperature increased to 150 °C, the emission intensity declined to 72%, 87%, 92% and 77% of their initial values at room temperature for $Ca_{0.97}AlSiN_3$:0.03Eu^{2+}@Eu_2O_3, $Ca_{0.97}AlSiN_3$:0.03Eu^{2+}@EuN, $Ca_{0.97}AlSiN_3$:0.03Eu^{2+}@EuB_6 as well as YAG:0.06Ce^{3+}, respectively.

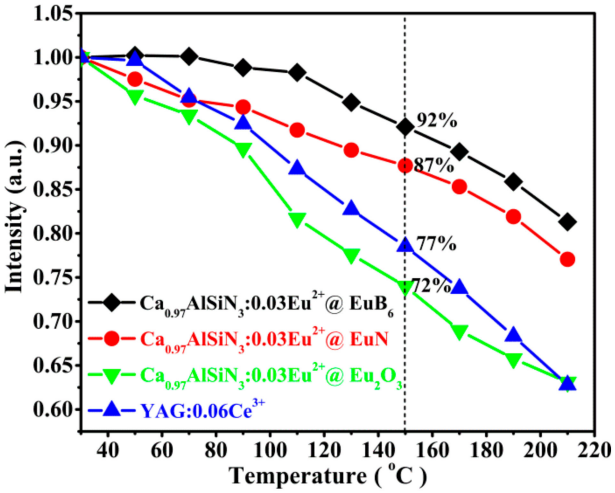

Figure 8. Temperature-dependent emission intensities of $Ca_{0.97}AlSiN_3$:0.03Eu^{2+}@Eu_2O_3 (green line), $Ca_{0.97}AlSiN_3$:0.03Eu^{2+}@EuN (red line), $Ca_{0.97}AlSiN_3$:0.03Eu^{2+}@EuB_6 (black line) and YAG:0.06Ce^{3+} (blue line) phosphors.

It is obvious that CASN:Eu^{2+}@EuB_6 has a preferable thermal stability than others. The increased thermal stability is attributable to the partial substitution of Eu–O (Eu–N) bonds by more covalent Eu–B ones that leads to a higher structural rigidity, which has already been observed in carbon-doped nitride phosphors [40–42]. Therefore, using nano-EuB_6 as a raw material in nitride luminescence materials can improve the luminescence performance as well as the thermal stability.

3.5. The Fabrication of W-LEDs Device

To demonstrate the potential application of the as-synthesized $Ca_{0.97}AlSiN_3$:0.03Eu^{2+}@EuB_6 red nitrides phosphor, a prototype of W-LEDs was fabricated by combining a 455 nm blue LED chip with a mixture of commercial green phosphor G3537 (produced by Dalian Luming) and the as-synthesized red phosphor $Ca_{0.97}AlSiN_3$:0.03Eu^{2+}@EuB_6. The normalized photoluminescence (PL) spectrum of the as-fabricated W-LEDs is shown in Figure 9. The corresponding CRI, CCT, luminous efficiency and CIE chromaticity coordinates were determined to be 95.8, 4989 K, 44.5 lm/W and (0.3460, 0.3577), respectively. The value of CRI is higher than that of traditional W-LED production made by combining yellow phosphor YAG:Ce^{3+} with blue LED chip (Ra ≈ 75). The W-LED packaging results indicate that the as-synthesized $Ca_{0.97}AlSiN_3$:0.03Eu^{2+}@EuB_6 is a potential candidate as a red phosphor for W-LEDs based on blue LEDs.

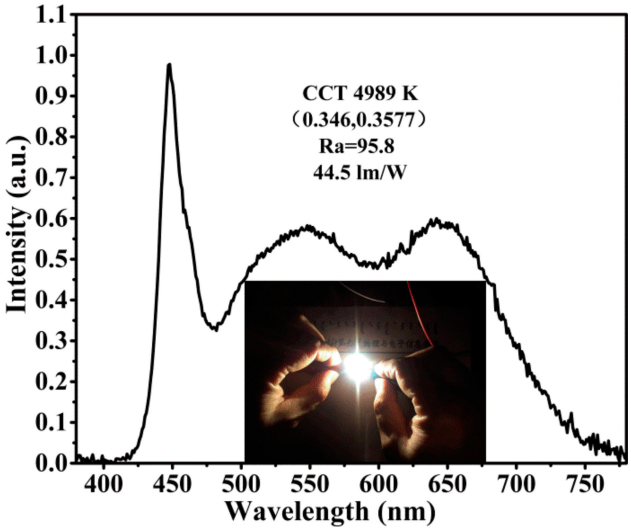

Figure 9. The normalized PL spectrum of a W-LED using a blue-LED chip (455 nm) and G3537 and $Ca_{0.97}AlSiN_3$:0.03Eu^{2+}@EuB_6 phosphors.

4. Conclusions

In this paper, three series of CASN:Eu^{2+} red nitride phosphors, using Eu_2O_3, EuN and EuB_6 as raw materials, were successfully synthesized by the alloy precursor normal pressure nitridation. The morphologies, crystal phases, compositions, XPS spectra as well as luminescence properties were investigated in detail. Interrelated Analysis of XPS indicates that the Eu^{2+} content in CASN:Eu^{2+}@EuB_6 is significantly higher than in CASN:Eu^{2+}@Eu_2O_3, thus it causes a stronger emission intensity of CASN:Eu^{2+}@EuB_6 than others. Furthermore, CASN:Eu^{2+}@EuB_6 has a preferable thermal stability is attributable to the partial substitution of Eu–O (Eu–N) bonds by more covalent Eu-B ones that leads to a higher structural rigidity. Consequently, nano-EuB_6 doped red nitride phosphor has the potential for application in high-power pc-LEDs and using nano-EuB_6 as raw material by the alloy precursor normal pressure nitridation method possesses the high advantage of relative low reaction temperature, cheap raw materials and simple processing.

Acknowledgments: Thanks for the financial support from the National Natural Science Foundation of China (Grant No. 51262022, 21663018), Inner Mongolia Autonomous Region Science and Technology Program (2015) and Inner Mongolia Autonomous Region Science and Technology Innovation Guide Award Fund (2016) funded topics.

Author Contributions: Ke-Fu Chao and Wen-Quan Liu conceived the experiments; Wen-Quan Liu designed, analyzed, and wrote the first draft of the paper; Dan Wu provided the language revision. All authors contributed to the discussion.

Conflicts of Interest: The authors declare no conflict of interest.

References

1. Kim, Y.H.; Arunkumar, P.; Kim, B.Y.; Unithrattil, S.; Kim, E.; Moon, S.H.; Hyun, J.Y.; Kim, K.H.; Lee, D.; Lee, J.S.; et al. A zero-thermal-quenching phosphor. *Nat. Mater.* **2017**, *16*, 543–550. [CrossRef] [PubMed]
2. Stanish, P.C.; Radovanovic, P.V. Energy Transfer between Conjugated Colloidal Ga_2O_3 and CdSe/CdS Core/Shell Nanocrystals for White Light Emitting Applications. *Nanomaterials* **2016**, *6*, 32. [CrossRef] [PubMed]
3. Zhong, J.; Zhao, W.; Zhuang, W.; Du, F.; Zhou, Y.; Yu, Y.; Wang, L. Selective coordination of N^{3-} and tuning of luminescence in garnet $(Y_{1-x},La_x)_3(Al,Si)_5(O,N)_{12}$:$Ce^{3+}$ phosphors. *J. Alloys Compd.* **2017**, *726*, 658–663. [CrossRef]
4. Wang, L.; Xie, R.-J.; Li, Y.; Wang, X.; Ma, C.-G.; Luo, D.; Takeda, T.; Tsai, Y.-T.; Liu, R.-S.; Hirosaki, N. $Ca_{1-x}Li_xAl_{1-x}Si_{1+x}N_3$:$Eu^{2+}$ solid solutions as broadband, color-tunable and thermally robust red phosphors for superior color rendition white light-emitting diodes. *Light Sci. Appl.* **2016**, *5*, e16155. [CrossRef]

5. Pan, F.; Zhou, M.; Zhang, J.; Zhang, X.; Wang, J.; Huang, L.; Kuang, X.; Wu, M. Double substitution induced tunable luminescent properties of $Ca_{3-x}Y_xSc_{2-x}Mg_xSi_3O_{12}:Ce^{3+}$ phosphors for white LEDs. *J. Mater. Chem. C* **2016**, *4*, 5671–5678. [CrossRef]
6. Li, X.; Budai, J.D.; Liu, F.; Howe, J.Y.; Zhang, J.; Wang, X.-J.; Gu, Z.; Sun, C.; Meltzer, R.S.; Pan, Z. New yellow $Ba_{0.93}Eu_{0.07}Al_2O_4$ phosphor for warm-white light-emitting diodes through single-emitting-center conversion. *Light Sci. Appl.* **2013**, *2*, e50. [CrossRef]
7. Xie, R.J.; Hirosaki, N.; Li, Y.; Takeda, T. Rare-Earth Activated Nitride Phosphors: Synthesis, Luminescence and Applications. *Materials* **2010**, *3*, 3777–3793. [CrossRef]
8. Zhang, W.T.; Wang, Y.L.; Gao, Y.; Long, J.P.; Li, J.F. Sol-gel assisted synthesis and photoluminescence property of $Sr_2Si_5N_8:Eu^{2+}$, Dy^{3+}red phosphor for white light emitting diodes. *J. Alloys Compd.* **2016**, *667*, 341–345. [CrossRef]
9. Suehiro, T.; Xie, R.J.; Hirosaki, N. Facile Synthesis of $(Sr,Ca)_2Si_5N_8:Eu^{2+}$-Based Red-Emitting Phosphor for Solid-State Lighting. *Ind. Eng. Chem. Res.* **2013**, *52*, 7453–7456. [CrossRef]
10. Li, H.L.; Xie, R.J.; Hirosaki, N.; Takeda, T.; Zhou, G.H. Synthesis and Luminescence Properties of Orange-Red-Emitting $M_2Si_5N_8:Eu^{2+}$(M=Ca, Sr, Ba) Light-Emitting Diode Conversion Phosphors by a Simple Nitridation of MSi_2. *Int. J. Appl. Ceram. Technol.* **2009**, *6*, 459–464. [CrossRef]
11. Chen, C.C.; Chen, W.J.; Rainwater, B.; Liu, L.X.; Zhang, H.L.; Liu, Y.X.; Guo, X.S.; Zhou, J.Y.; Xie, E.Q. $M_2Si_5N_8:Eu^{2+}$-based (M=Ca, Sr) red-emitting phosphors fabricated by nitrate reduction process. *Opt. Mater.* **2011**, *33*, 1585–1590. [CrossRef]
12. Tsai, Y.T.; Nguyen, H.D.; Lazarowska, A.; Mahlik, S.; Grinberg, M.; Liu, R.S. Improvement of the Water Resistance of a Narrow-Band Red-Emitting $SrLiAl_3N_4:Eu^{2+}$Phosphor Synthesized under High Isostatic Pressure through Coating with an Organosilica Layer. *Angew. Chem.* **2016**, *55*, 9652–9656. [CrossRef] [PubMed]
13. Zhang, X.; Tsai, Y.T.; Wu, S.M.; Lin, Y.C.; Lee, J.F.; Sheu, H.S.; Cheng, B.M.; Liu, R.S. Facile Atmospheric Pressure Synthesis of High Thermal Stability and Narrow-Band Red-Emitting $SrLiAl_3N_4:Eu^{2+}$ Phosphor for High Color Rendering Index White Light-Emitting Diodes. *ACS Appl. Mater. Interfaces* **2016**, *8*, 19612–19617. [CrossRef] [PubMed]
14. Cui, D.; Xiang, Q.; Song, Z.; Xia, Z.; Liu, Q. The synthesis of narrow-band red-emitting $SrLiAl_3N_4:Eu^{2+}$ phosphor and improvement of its luminescence properties. *J. Mater. Chem. C* **2016**, *4*, 7332–7338. [CrossRef]
15. Kim, S.W.; Hasegawa, T.; Hasegawa, S.; Yamanashi, R.; Nakagawa, H.; Toda, K.; Ishigaki, T.; Uematsu, K.; Sato, M. Improved synthesis of $SrLiAl_3N_4:Eu^{2+}$ phosphor using complex nitride raw material. *RSC Adv.* **2016**, *6*, 61906–61908. [CrossRef]
16. Chen, L.; Fei, M.; Zhang, Z.; Jiang, Y.; Chen, S.; Dong, Y.; Sun, Z.; Zhao, Z.; Fu, Y.; He, J.; et al. Understanding the Local and Electronic Structures toward Enhanced Thermal Stable Luminescence of $CaAlSiN_3:Eu^{2+}$. *Chem. Mater.* **2016**, *28*, 5505–5515. [CrossRef]
17. Yang, J.J.; Wang, T.; Chen, D.C.; Chen, G.D.; Liu, Q.L. An investigation of Eu^{2+}-doped $CaAlSiN_3$ fabricated by an alloy-nitridation method. *Mater. Sci. Eng. B* **2012**, *177*, 1596–1604. [CrossRef]
18. Li, J.W.; Watanabe, T.; Sakamoto, N.; Wada, H.; Setoyama, T.; Yoshimura, M. Synthesis of a Multinary Nitride, Eu-Doped $CaAlSiN_3$, from Alloy at Low Temperatures. *Chem. Mater.* **2008**, *20*, 2095–2105. [CrossRef]
19. Piao, X.; Machida, K.; Horikawa, T.; Hanzawa, H.; Shimomura, Y.; Kijima, N. Preparation of $CaAlSiN_3:Eu^{2+}$ phosphors by the self-propagating high-temperature synthesis and their luminescent properties. *Chem. Mater.* **2007**, *19*, 4592–4599. [CrossRef]
20. Cai, C.; Qian, J.; Zhang, B.; Hu, W.; Hao, L.; Xu, X.; Wang, Y. Synthesis of Red-Emitting $CaAlSiN_3:Eu^{2+}$ Phosphors through a Cost-Effective Synthetic Route. *ECS J. Solid State Sci. Technol.* **2014**, *3*, R169–R172. [CrossRef]
21. Dierre, B.; Takeda, T.; Sekiguchi, T.; Suehiro, T.; Takahashi, K.; Yamamoto, Y.; Xie, R.J.; Hirosaki, N. Local analysis of Eu^{2+} emission in $CaAlSiN_3$. *Sci. Technol. Adv. Mater.* **2013**, *14*, 064201. [CrossRef] [PubMed]
22. Kim, Y.S.; Choi, S.W.; Park, J.H.; Bok, E.; Kim, B.K.; Hong, S.H. Red-Emitting $(Sr,Ca)AlSiN_3:Eu^{2+}$ Phosphors Synthesized by Spark Plasma Sintering. *Ecs J. Solid State Sci. Technol.* **2013**, *2*, R3021–R3025. [CrossRef]
23. Kim, B.H.; Kang, E.H.; Choi, S.W.; Hong, S.H. Luminescence properties of $La_2Si_6O_3N_8:Eu^{2+}$phosphors prepared by spark plasma sintering. *Opt. Mater.* **2013**, *36*, 182–185. [CrossRef]

24. Chung, S.L.; Huang, S.C. Synthesis of $CaAlSiN_3:Eu^{2+}$ Phosphor via the Self-Propagating High Temperature Synthesis Method and its Optical Properties. *Adv. Mater. Res.* **2014**, *904*, 33–35. [CrossRef]
25. Li, S.X.; Peng, X.; Liu, X.J.; Huang, Z.R. Photoluminescence of $CaAlSiN_3:Eu^{2+}$-based fine red-emitting phosphors synthesized by carbothermal reduction and nitridation method. *Opt. Mater.* **2014**, *38*, 242–247. [CrossRef]
26. Li, S.X.; Liu, X.J.; Mao, R.H.; Huang, Z.R.; Xie, R.J. Red-emission enhancement of the $CaAlSiN_3:Eu^{2+}$ phosphor by partial substitution for Ca_3N_2 by $CaCO_3$and excess calcium source addition. *RSC Adv.* **2015**, *5*, 76507–76515. [CrossRef]
27. Li, S.X.; Liu, X.J.; Liu, J.Q.; Li, H.L.; Mao, R.H.; Huang, Z.R.; Xie, R.J. Synthesis, composition optimization, and tunable red emission of $CaAlSiN_3:Eu^{2+}$ phosphors for white light-emitting diodes. *J. Mater. Res.* **2015**, *30*, 2919–2927. [CrossRef]
28. Kim, H.S.; Horikawa, T.; Hanzawa, H.; Machida, K.-I. Luminescence properties of $CaAlSiN_3:Eu^{2+}$ mixed nitrides prepared by carbothermal process. *J. Phys. Conf. Ser.* **2012**, *379*, 012016. [CrossRef]
29. Aronson, M.C. Fermi surface of the ferromagnetic semimetal, EuB_6. *Phys. Rev. B* **1999**, *59*, 4720–4724. [CrossRef]
30. Manna, R.S.; Das, P.; de Souza, M.; Schnelle, F.; Lang, M.; Muller, J.; von Molnar, S.; Fisk, Z. Lattice strain accompanying the colossal magnetoresistance effect in EuB_6. *Phys. Rev. Lett.* **2014**, *113*, 672021–672025. [CrossRef] [PubMed]
31. Bao, L.; Wurentuya, B.; Wei, W.; Li, Y.; Tegus, O. Chemical synthesis and microstructure of nanocrystalline RB_6 (R = Ce, Eu). *J. Alloys Compd.* **2014**, *617*, 235–239.
32. Kim, H.S.; Machida, K.; Horikawa, T.; Hanzawa, H. Luminescence properties of $CaAlSiN_3:Eu^{2+}$ phosphor prepared by direct-nitriding method using fine metal hydride powders. *J. Alloys Compd.* **2015**, *633*, 97–103. [CrossRef]
33. Li, G.; Zhao, Y.; Xu, J.; Mao, Z.; Chen, J.; Wang, D. Effective suppression of AlN impurity in synthesis of $CaAlSiN_3:Eu^{2+}$ phosphors under condition of atmospheric pressure. *Mater. Chem. Phys.* **2017**, *201*, 1–6. [CrossRef]
34. Qi, J.F.; Matsumoto, T.; Tanaka, M.; Masumoto, Y. Europium silicate thin films on Si substrates fabricated by a radio frequency sputtering method. *J. Phys. D Appl. Phys.* **2000**, *33*, 2074–2078. [CrossRef]
35. Cho, E.J.; Oh, S.J. Surface valence transition in trivalent Eu insulating compounds observed by photoelectron spectroscopy. *Phys. Rev. B* **1999**, *59*, R15613–R15616. [CrossRef]
36. Riviere, J.P.; Pacaud, Y.; Cahoreau, M. Spectroscopic Studies of BN Films Deposited by Dynamic Ion Mixing. *Thin Solid Films* **1993**, *227*, 44–53. [CrossRef]
37. Beshkov, G.; Spassov, D.; Krastev, V.; Stefanov, P.; Georgiev, S.; Nemska, S. XPS study of BN_x nanolayers prepared by low pressure rapid thermal annealing in ammonia. *J. Phys. Conf. Ser.* **2008**, *113*, 012046. [CrossRef]
38. Ye, S.; Xiao, F.; Pan, Y.X.; Ma, Y.Y.; Zhang, Q.Y. Phosphors in phosphor-converted white light-emitting diodes: Recent advances in materials, techniques and properties. *Mater. Sci. Eng. R* **2010**, *71*, 1–34. [CrossRef]
39. Liu, W.Q.; Chao, K.F.; Wu, W.J.; Bao, F.Q.; Zhou, B.Q. $CaAlSiN_3:Eu^{2+}$ red phosphors synthesized by atmospheric nitrogen and their luminescence properties. *Acta Phys. Sin.* **2016**, *65*, 207801–207807.
40. Tian, Y. Development of phosphors with high thermal stability and efficiency for phosphor-converted LEDs. *J. Solid State Light.* **2014**, *1*, 1–15. [CrossRef]
41. Wang, L.; Wang, X.; Takeda, T.; Hirosaki, N.; Tsai, Y.T.; Liu, R.S.; Xie, R.J. Structure, Luminescence, and Application of a Robust Carbidonitride Blue Phosphor ($Al_{1-x}Si_xC_xN_{1-x}:Eu^{2+}$) for Near UV-LED Driven Solid State Lighting. *Chem. Mater.* **2015**, *27*, 8457–8466. [CrossRef]
42. Huang, W.Y.; Yoshimura, F.; Ueda, K.; Pang, W.K.; Su, B.J.; Jang, L.Y.; Chiang, C.Y.; Zhou, W.; Duy, N.H.; Liu, R.S. Domination of second-sphere shrinkage effect to improve photoluminescence of red nitride phosphors. *Inorg. Chem.* **2014**, *53*, 12822–12831. [CrossRef] [PubMed]